

Thermodynamic properties of nuclear “pasta” in neutron star crusts

Gentaro Watanabe^a, Kei Iida^{a,b}, Katsuhiko Sato^{a,c}

^a*Department of Physics, University of Tokyo, 7-3-1 Hongo, Bunkyo, Tokyo 113-0033, Japan*

^b*Department of Physics, University of Illinois at Urbana-Champaign, 1110 West Green Street, Urbana, IL 61801-3080, USA*

^c*Research Center for the Early Universe, University of Tokyo, 7-3-1 Hongo, Bunkyo, Tokyo 113-0033, Japan*

December 2, 2024

Abstract

Equilibrium phase diagrams for neutron star matter at subnuclear densities are obtained at zero temperature. Spherical, rod-like and slab-like nuclei as well as spherical and rod-like nuclear bubbles are taken into account by using a compressible liquid-drop model. This model is designed to incorporate uncertainties in the nuclear surface tension and in the proton chemical potential in a gas of dripped neutrons. The resultant phase diagrams show that for typical values of these quantities, the phases with rod-like nuclei and with slab-like nuclei occur in the form of Coulomb lattice at densities below a point where the system becomes uniform. Thermal fluctuations leading to displacements of such nuclei from their equilibrium positions are considered through explicit evaluations of their elastic constants; these fluctuations can be effective at destroying the layered lattice of slab-like nuclei in the temperature region typical of matter in the neutron star crust.

PACS : 26.60.+c; 97.60.Jd

Keywords : Dense matter; Ground state; Thermal fluctuations; Neutron stars

1 Introduction

In the outer part of a neutron star, nuclei are considered to mainly determine the state of matter in equilibrium [1]. Except for a thin envelope of the star, due to Coulomb interactions, nuclei form a bcc lattice neutralized by a roughly uniform sea of electrons. With increasing density, weak interactions render nuclei neutron-rich via electron captures. Then, at a density of about $\sim 4 \times 10^{11} \text{ g cm}^{-3}$, neutrons begin to drip out of these nuclei. The crystalline region of the star (not) including a gas of the dripped neutrons is usually referred to as an inner (outer) crust. In the deepest region of the inner crust, corresponding to densities just below the normal saturation density $\rho_s \sim 3 \times 10^{14} \text{ g cm}^{-3}$, not only are nuclei expected to have rod-like and slab-like shapes, but also the system is expected to turn inside out in such a way that the constituents of the original nuclei form a liquid containing rod-like and roughly spherical bubbles of the dripped neutrons. These transformations, as originally indicated by Ravenhall et al. [2] and Hashimoto et al. [3], stem from a delicate competition between the nuclear surface and Coulomb energies at small internuclear spacings.

Recent calculations of the ground state of matter in the crust, performed by using specific nuclear models [4, 5, 6], indicate that at a density of order $10^{13} \text{ g cm}^{-3}$, rather small compared with ρ_s , roughly spherical nuclei turn into elongated rod-like nuclei. Accordingly, the lattice structure is changed from a regular bcc lattice to a two-dimensional triangular lattice. With further increasing density, these rod-like nuclei are transformed into slab-like nuclei, which are arranged in the form of a layered lattice. After that, a two-dimensional triangular lattice of rod-like bubbles and a bcc Coulomb lattice of roughly

spherical bubbles appear in turn. At last, at a density of about $\rho_s/2$, the system dissolves into uniform nuclear matter. Since slabs and rods look like “lasagna” and “spaghetti”, the phases with positional order of one- and two-dimension are often referred to as “pasta” phases.

It is of interest to note the relevance of non-spherical nuclei to pulsar glitches and cooling of neutron stars. Pulsar glitches are usually considered to be manifestation of a sudden large-scale release of neutron vortices trapped by some pinning centers in the crust [7]. The force needed to pin vortices has yet to be clarified completely even for a bcc lattice of spherical nuclei due mainly to the uncertain properties of impurities and defects which may be involved in the vortex pinning [8]. Whether or not neutron vortex pinning occurs in the “pasta” phases possibly formed depends also on the unknown properties of impurities and defects in the lattice. The presence of non-spherical nuclei would accelerate the cooling of neutron stars by opening semi-leptonic weak processes which are unlikely to occur for spherical nuclei [4]. This stems from the fact that in non-spherical nuclei, protons have a continuous spectrum at the Fermi surface in the elongated direction.

At what densities the phases with non-spherical nuclei and with bubbles are energetically more favorable than the usual bcc phase and the phase of uniform nuclear matter depends on the properties of neutron-rich nuclei and of the surrounding pure neutron gas. The quantities that mainly describe such properties but are still uncertain are the nuclear surface tension E_{surf} and the energy required to add a proton to the pure neutron gas, i.e., the proton chemical potential $\mu_p^{(0)}$. E_{surf} controls the size of the nuclei and bubbles, and hence the sum of the electrostatic and interfacial energies. With increasing E_{surf} and so

this energy sum, the density ρ_m at which the system becomes uniform is lowered. There is also a tendency that the lower $\mu_p^{(0)}$, the smaller ρ_m . This is because $-\mu_p^{(0)}$ represents the degree to which the neutron gas favors the presence of protons in itself. This feature is implied by the work of Arponen [9] who studied the sensitivity of the properties of uniform nuclear matter at low proton fraction to the melting density ρ_m . Although E_{surf} and $\mu_p^{(0)}$ have not been fully determined, previous authors (e.g., Refs. [4, 5, 6]) designated the values of these quantities almost uniquely. In this paper, by generalizing a compressible liquid-drop model developed by Baym, Bethe and Pethick [10] (hereafter denoted by BBP) in such a way as to incorporate uncertainties in E_{surf} and $\mu_p^{(0)}$, we draw the equilibrium phase diagrams of zero-temperature neutron star matter at subnuclear densities. The resulting phase diagrams show that while the phases with rod-like bubbles and with spherical bubbles can exist only for unrealistically low E_{surf} , the phases with rod-like nuclei and with slab-like nuclei survive almost independently of E_{surf} and $\mu_p^{(0)}$.

For these two phases, there are directions in which the system is translationally invariant. As noted by Pethick and Potekhin [11], this situation is geometrically analogous with a liquid crystal rather than with a rigid solid. Elastic properties of the nuclear rods and slabs are thus characterized by elastic constants used for the corresponding liquid-crystal phases, i.e., columnar phases and smectics A, respectively. They expressed such constants in terms of the interfacial and Coulomb energies. These energies, as well as the energies of bulk nucleon matter and of an electron gas, are well described by the zero-temperature approximation. This is because the temperature of the crust $\lesssim 10^9$ K, as inferred from X-ray observations of rotation-powered pulsars, is small compared with typical nuclear and

electronic excitation energies. However, such temperature may have consequence to the structure of the Coulomb lattices involved. For example, the outer boundary of the crust is acutely controlled by the temperature because of the density dependence of the melting temperature of the bcc lattice [12]. In the deepest region of the crust, thermal fluctuations may possibly spoil the ordering sustained by the layered and triangular lattices, as expected from the usual Landau-Peierls argument. We thus calculate thermally induced displacements of non-spherical nuclei by using the elastic constants given by Pethick and Potekhin [11]. The critical temperatures at which the ordered structure is destroyed by the thermal fluctuations are also estimated.

In Section 2 we construct a compressible liquid-drop model for nuclei and bubbles, and we write down equilibrium conditions for zero-temperature matter in the crust. The resultant phase diagrams are displayed in Section 3. Properties of the phase transitions involved are discussed in Section 4. In Section 5 displacements of rod-like and slab-like nuclei are calculated at finite temperatures. Conclusions are given in Section 6.

2 Model for neutron star matter at subnuclear densities

In this section, we write the energy of zero-temperature matter in the crust and the conditions for its equilibrium. We consider five phases which contain spherical nuclei, cylindrical nuclei, planar nuclei, cylindrical bubbles and spherical bubbles, respectively. Each phase is taken to be composed of a single species of nucleus or bubble at a given baryon density n_b . Crystalline structures of these phases are taken into account in the

Wigner-Seitz approximation, which leads to sufficiently accurate evaluations of the lattice energy [5]. In this approximation, a cell in the bcc lattice, including a spherical nucleus or bubble of radius r_N , is replaced by a Wigner-Seitz cell defined as a sphere having radius r_c and the same center. A cylindrical nucleus or bubble having an infinitely long axis and a circular section of radius r_N is taken to be contained in a cylindrical Wigner-Seitz cell having the same axis and a circular section of radius r_c in place of a cell in the two-dimensional triangular lattice. For a planar nucleus with width $2r_N$, a cell in the one-dimensional layered lattice, having width $2r_c$, is identified with the corresponding Wigner-Seitz cell. The values of r_c for these phases are chosen so that each Wigner-Seitz cell may have zero net charge and hence have the same volume as that of the original cell.

2.1 Energy of matter

For the purpose of constructing a formula for the energy of the system allowing for uncertainties in E_{surf} and $\mu_p^{(0)}$, a compressible liquid-drop model for nuclei and bubbles is of practical use, which is characterized by the energy densities of uniform nuclear matter and neutron matter as well as by the interfacial and Coulomb energies. In this model, neutrons and protons are assumed to be distributed uniformly inside and outside the nuclei or bubbles. A sea of electrons, which ensures the charge neutrality of the system, is taken to be homogeneous. We thus write the total energy density E_{tot} as

$$E_{\text{tot}} = \begin{cases} w_N + w_L + (1-u)E_n(n_n) + E_e(n_e) & \text{(nuclei)} , \\ w_N + w_L + uE_n(n_n) + E_e(n_e) & \text{(bubbles)} , \end{cases} \quad (1)$$

where w_N is the energy of the nuclear matter region in a cell as divided by the cell volume, w_L is the lattice energy per unit volume as given for the finite-size nuclei or bubbles, n_n is

the number density of neutrons outside the nuclei or inside the bubbles, n_e is the number density of the electrons, E_n and E_e are the energy densities of the neutron matter and of the electron gas, respectively, and u is the volume fraction occupied by the nuclei or bubbles,

$$u = \left(\frac{r_N}{r_c} \right)^d = \begin{cases} \frac{n_b - n_n}{n - n_n} & \text{(nuclei)} , \\ \frac{n - n_b}{n - n_n} & \text{(bubbles)} , \end{cases} \quad (2)$$

where d is the dimensionality defined as $d = 1$ for slabs, $d = 2$ for cylinders and $d = 3$ for spheres, and n is the nucleon number density in the nuclear matter region. In Eq. (1), we ignore corrections due to nucleon pairing effects, shell and curvature effects in the nuclei and bubbles, and deformations and surface diffuseness of the nuclei and bubbles.

In writing w_N , we adopt a generalized version of the compressible liquid drop model developed by BBP [10]. w_N is then expressed as

$$w_N(n, x, n_n, r_N, r_c, d) = \begin{cases} un[(1-x)m_n + xm_p]c^2 + unW(k, x) \\ \quad + w_{\text{surf}}(n, x, n_n, r_N, u, d) + w_C(n, x, r_N, u, d) & \text{(nuclei)} , \\ (1-u)n[(1-x)m_n + xm_p]c^2 + (1-u)nW(k, x) \\ \quad + w_{\text{surf}}(n, x, n_n, r_N, u, d) + w_C(n, x, r_N, u, d) & \text{(bubbles)} , \end{cases} \quad (3)$$

where m_n (m_p) is the neutron (proton) rest mass, $W(k, x)$ is the energy per nucleon for uniform nuclear matter of nucleon Fermi wave number $k = (3\pi^2 n/2)^{1/3}$ and proton fraction x , as given by BBP [see Eq. (3.19) in Ref. [10]], w_{surf} is the nuclear surface energy per unit volume, and w_C is the self Coulomb energy (per unit volume) of protons contained in a cell.

$W(k, x)$ includes four parameters characterizing the saturation properties of nearly symmetric nuclear matter, which are the binding energy w_0 , the saturation density $2k_0^3/3\pi^2$,

the incompressibility K and the coefficient s determining the symmetry energy. In the present work, the values for these parameters determined empirically by BBP in such a way as to reproduce nuclear masses and radii of β stable nuclei are replaced by the following values that are generally accepted among recent literature: $w_0 = 16.0$ MeV, $k_0 = 1.36$ fm $^{-1}$, $K = 230$ MeV and $s = 30.0$ MeV. We remark in passing that such a replacement makes no significant difference in the phase diagrams for neutron star matter at subnuclear densities that will be exhibited in Section 3.

The proton chemical potential $\mu_p^{(0)}$ in pure neutron matter is contained in $W(k, x)$. This quantity, dominating stability of the phases including a dripped neutron gas over the phase of uniform nuclear matter, has not been well determined from microscopic calculations based on nucleon-nucleon interactions. We thus set $\mu_p^{(0)}$ (not including the rest mass) as

$$\mu_p^{(0)} = -C_1 n_n^{2/3} , \quad (4)$$

where C_1 is the free parameter being positive definite. As can be seen from Fig. 1, Eq. (4) approximately reproduces the overall density dependence of the results obtained from the Hartree-Fock theory with Skyrme interactions (see Ref. [13] and references therein) and from the lowest-order Brueckner theory with the Reid soft-core potential [14, 15]. Hereafter, C_1 will be set as $C_1 = 300, 400, 500, 600$ MeV fm 2 ; the case of $C_1 = 300$ MeV fm 2 agrees well with the result of Siemens and Pandharipande [14] adopted by BBP, whereas the case of $C_1 = 400$ MeV fm 2 is consistent with the other results cited in Fig. 1 for densities of interest to us $n \lesssim 0.12$ fm $^{-3}$.

In constructing the surface energy per unit volume w_{surf} , we take note of the expression

given by BBP [see Eq. (4.30) in Ref. [10]] and the Hartree-Fock calculations by Ravenhall, Bennett and Pethick [16] (hereafter denoted by RBP) using a Skyrme interaction. For comparison, it is useful to consider the surface tension E_{surf} that is independent of the shapes of nuclei and bubbles; this is related to w_{surf} via

$$E_{\text{surf}} = \frac{r_N w_{\text{surf}}}{ud} . \quad (5)$$

Following the spirit of Iida and Sato [17], we express E_{surf} as

$$E_{\text{surf}} = C_2 \tanh \left(\frac{C_3}{\mu_n^{(0)}} \right) E_{\text{surf}}^{\text{BBP}} , \quad (6)$$

where C_2 and C_3 are the adjustable parameters that will be discussed just below, $\mu_n^{(0)} = \partial E_n / \partial n_n - m_n c^2$ is the neutron chemical potential in the neutron gas not including the rest mass, and

$$E_{\text{surf}}^{\text{BBP}} = \frac{\sigma(n - n_n)^{2/3} [W(k_n, 0) - W(k, x)]}{(36\pi^{1/3} w_0)} , \quad (7)$$

with $k_n = (3\pi^2 n_n / 2)^{1/3}$ and $\sigma = 21.0$ MeV. If we set $C_2 = 1.0$ and $C_3 = 3.5$ MeV for $C_1 = 400$ MeV fm², as shown in Fig. 2, the surface tension calculated for matter in equilibrium (see Subsection 2.2 for details) agrees well with the RBP values for proton fractions of interest here $x \lesssim 0.2$. For $C_1 = 300, 500, 600$ MeV fm², consistency with the RBP values is also obtained from $C_2 = 1.0$ and $C_3 = 3.5$ MeV. Hereafter this value of C_3 will be fixed, whereas, for our present purpose of examining the dependence on nuclear models of the equilibrium phase diagrams for matter in the crust, we shall shake the values of C_2 within a rather wide range covering $C_2 = 1.0$ (see Section 3).

We proceed to express the total electrostatic energy per unit volume $w_{\text{C+L}} = w_{\text{C}} + w_{\text{L}}$.

In the Wigner-Seitz approximation adopted here, it reads [1]

$$w_{C+L} = 2\pi(exnr_N)^2 u f_d(u) , \quad (8)$$

with

$$f_d(u) = \frac{1}{d+2} \left[\frac{2}{d-2} \left(1 - \frac{du^{1-2/d}}{2} \right) + u \right] . \quad (9)$$

The energy density of the pure neutron gas, whose density derivative $\mu_n^{(0)}$, together with E_{surf} and $\mu_p^{(0)}$, plays a role in determining the melting density ρ_m [13], is set by using $W(k, x)$ as

$$E_n(n_n) = [W(k_n, 0) + m_n c^2] n_n . \quad (10)$$

Note that this energy density corresponds to the fitting formula determined by BBP [see Eq. (3.8) in Ref. [10]] so as to reproduce the data for $k_n \lesssim 1.7 \text{ fm}^{-3}$ obtained by Siemens and Pandharipande [14] in the lowest-order Brueckner theory with the Reid soft-core potential. These data hold good at least for $k_n \lesssim k_0$, as can be seen from comparison with the results from several works based on more elaborate many-body schemes and potential models [13]. We shall thus use the BBP formula without any modification.

The energy density of the free electron gas, which is relativistic and degenerate, is finally expressed as

$$E_e(n_e) = \frac{3}{4} \hbar c k_e n_e , \quad (11)$$

with the electron Fermi wave number $k_e = (3\pi^2 n_e)^{1/3}$. Here, we ignore the electron mass and the electron Hartree-Fock energy.

2.2 Equilibrium conditions

As a next step towards the description of the equilibrium phase diagrams for crustal matter, we minimize the energy density E_{tot} with respect to five variables n , x , n_{n} , r_{N} and u under fixed baryon density n_{b} ,

$$n_{\text{b}} = \begin{cases} un + (1 - u)n_{\text{n}} & \text{(nuclei)} , \\ (1 - u)n + un_{\text{n}} & \text{(bubbles)} . \end{cases} \quad (12)$$

and under charge neutrality,

$$n_{\text{e}} = \begin{cases} xnu & \text{(nuclei)} , \\ xn(1 - u) & \text{(bubbles)} . \end{cases} \quad (13)$$

Such minimization results in four equilibrium conditions, which were given by BBP for spherical nuclei (see Section 2 in Ref. [10]).

Optimization of E_{tot} with respect to r_{N} at fixed n , x , n_{n} and u leads to a familiar relation for size-equilibrium,

$$w_{\text{surf}} = 2w_{\text{C+L}} . \quad (14)$$

This relation is thus independent of dimensionality d . Such independence was understood [1] from the fact that the system, no matter what type of nucleus or bubble it may contain, is in a three-dimensional physical space.

The condition for equilibrium of the dripped neutrons with the neutrons in the nuclear matter region, arising from minimization of E_{tot} with respect to n at fixed n_{b} , nx , r_{N} and u , reads

$$\mu_{\text{n}}^{(\text{N})} = \mu_{\text{n}}^{(\text{G})} . \quad (15)$$

Here

$$\mu_n^{(N)} = \begin{cases} \frac{\partial(w_N + w_L)}{u \partial n} \Big|_{nx, n_n, r_N, u} - m_n c^2 & \text{(nuclei)} \\ \frac{1}{1-u} \frac{\partial(w_N + w_L)}{\partial n} \Big|_{nx, n_n, r_N, u} - m_n c^2 & \text{(bubbles)} \end{cases} \quad (16)$$

is the neutron chemical potential in the nuclear matter region, and

$$\mu_n^{(G)} = \begin{cases} \left(\frac{\partial E_n}{\partial n_n} - m_n c^2 \right) + \frac{1}{1-u} \frac{\partial w_N}{\partial n_n} \Big|_{n, x, r_N, u} & \text{(nuclei)} \\ \left(\frac{\partial E_n}{\partial n_n} - m_n c^2 \right) + \frac{1}{u} \frac{\partial w_N}{\partial n_n} \Big|_{n, x, r_N, u} & \text{(bubbles)} \end{cases} \quad (17)$$

is the neutron chemical potential in the neutron gas modified by the surface energy.

The condition that the nuclear matter region is stable against β -decay is yielded by minimization of E_{tot} with respect to x at fixed n , n_n , r_N and u . It is expressed as

$$\mu_e - (m_n - m_p)c^2 = \mu_n^{(N)} - \mu_p^{(N)}, \quad (18)$$

where

$$\mu_e = \hbar k_e c \quad (19)$$

is the electron chemical potential, and

$$\mu_p^{(N)} = \begin{cases} \frac{\partial(w_N + w_L)}{u \partial(nx)} \Big|_{n(1-x), n_n, r_N, u} - m_p c^2 & \text{(nuclei)} \\ \frac{1}{1-u} \frac{\partial(w_N + w_L)}{\partial(nx)} \Big|_{n(1-x), n_n, r_N, u} - m_p c^2 & \text{(bubbles)} \end{cases} \quad (20)$$

is the proton chemical potential in the nuclear matter region.

Finally, minimizing E_{tot} with respect to r_N at fixed un , x , r_c and $(1 - u)n_n$ for nuclei [$(1 - u)n$, x , r_c and un_n for bubbles] yields the condition for pressure equilibrium between the nuclear matter and the neutron gas,

$$P^{(N)} = P^{(G)} , \quad (21)$$

where

$$P^{(N)} = \begin{cases} -\frac{\partial(w_N + w_L)}{\partial u} \Big|_{nu, x, n_n, r_c} & \text{(nuclei)} \\ \frac{\partial(w_N + w_L)}{\partial u} \Big|_{n(1-u), x, n_n, r_c} & \text{(bubbles)} \end{cases} \quad (22)$$

is the pressure of the nuclear matter region, and

$$P^{(G)} = n_n [\mu_n^{(G)} - W(k_n, 0)] \quad (23)$$

is the pressure of the neutron gas.

At given n_b and subject to charge neutrality (13), we have calculated the total energy density E_{tot} for the five phases containing spherical nuclei, cylindrical nuclei, planar nuclei, spherical bubbles and cylindrical bubbles, respectively. In such calculations, we first express x , r_N and r_c in terms of n_b , n and n_n by using conditions (12), (14) and (18). In this stage, we can rewrite $\mu_n^{(N)}$, $\mu_n^{(G)}$ and $P^{(N)}$ given by Eqs. (16), (17) and (22) as

$$\mu_n^{(N)} = \begin{cases} W(k, x) + \frac{k}{3} \frac{\partial W(k, x)}{\partial k} + \frac{d}{r_N} \left(\frac{1}{n} + \frac{\partial}{\partial n} \right) E_{\text{surf}} + x[\mu_e - (m_n - m_p)c^2] & \text{(nuclei)} , \\ W(k, x) + \frac{k}{3} \frac{\partial W(k, x)}{\partial k} + \frac{d}{r_N} \left(\frac{u}{1-u} \right) \left(\frac{1}{n} + \frac{\partial}{\partial n} \right) E_{\text{surf}} + x[\mu_e - (m_n - m_p)c^2] & \text{(bubbles)} , \end{cases} \quad (24)$$

$$\mu_n^{(G)} = \begin{cases} W(k_n, 0) + \frac{k_n}{3} \frac{\partial W(k_n, 0)}{\partial k_n} + \frac{d}{r_N} \frac{u}{1-u} \frac{\partial E_{\text{surf}}}{\partial n_n} & \text{(nuclei)} , \\ W(k_n, 0) + \frac{k_n}{3} \frac{\partial W(k_n, 0)}{\partial k_n} + \frac{d}{r_N} \frac{\partial E_{\text{surf}}}{\partial n_n} & \text{(bubbles)} , \end{cases} \quad (25)$$

$$P^{(N)} = \begin{cases} \frac{nk}{3} \frac{\partial W(k, x)}{\partial k} - \frac{d-1}{r_N} E_{\text{surf}} + \frac{dn}{r_N} \frac{\partial E_{\text{surf}}}{\partial n} + \frac{4\pi r_N^2}{d(d+2)} (exn)^2 (1-u) & \text{(nuclei)} , \\ \frac{nk}{3} \frac{\partial W(k, x)}{\partial k} + \frac{d-1}{r_N} E_{\text{surf}} + \frac{dn}{r_N} \frac{u}{1-u} \frac{\partial E_{\text{surf}}}{\partial n} - \frac{4\pi r_N^2}{d(d+2)} (exn)^2 (1-u) & \text{(bubbles)} . \end{cases} \quad (26)$$

Conditions (15) and (21) in turn give n and n_n as function of n_b . Substitution of these values into Eq. (1) leads thus to the minimum values of E_{tot} at given n_b and conformation. The energy density for β -equilibrated uniform nuclear matter has also been evaluated at the same n_b by using the energy densities $nW(k, x)$ and $E_e(n_e)$ and by following a line of argument of BBP (see Section 8 in Ref. [10]). Here we ignore the presence of muons, the number density of which is, if any, far smaller than n_e for densities of interest here. We have finally found the phase giving the smallest energy density among the uniform and crystalline phases; the resultant phase diagrams for the ground-state matter at subnuclear densities will be shown in the next section.

3 Phase diagrams

We may now draw the phase diagrams for neutron star matter in the ground state on the n_b versus C_2 plane for $C_1 = 300, 400, 500, 600$ MeV fm 2 .¹ The results have been plotted in Fig. 3. We have thus confirmed the tendency, as mentioned in Section 1, that larger E_{surf} and lower $\mu_p^{(0)}$ help the uniform matter phase “erode” the phases with non-spherical nuclei and with bubbles.

As can be found from Fig. 3, the obtained phase diagrams basically reproduce the

¹Note that these diagrams are different from the usual ones written over the density versus temperature plane.

feature that with increasing density, the shape of the nuclear matter region changes like sphere → cylinder → slab → cylindrical hole → spherical hole → uniform matter. This feature can be derived from simple discussions about the Coulomb and surface effects ignoring the bulk energy [3]. However, it is significant to notice that for most sets of C_1 and C_2 including the typical one ($C_1 = 400$ MeV fm 2 and $C_2 = 1.0$), the shape changes become simpler, i.e., sphere → cylinder → slab → uniform matter. This behavior, due probably to bulk corrections to the Coulomb and surface effects, was not observed in the previous works (see, e.g., Refs. [4, 5, 6]). Since the values of E_n , $\mu_p^{(0)}$ and E_{surf} as adopted by these works are consistent with those obtained here for $C_1 = 400$ MeV fm 2 and $C_2 = 1.0$, we may conclude that the difference in the phase diagrams should originate mainly from that in the properties of uniform nuclear matter at low but *finite* proton fractions, i.e., $x \sim 0.1$. These properties depend on the adopted schemes for constructing interpolation between almost pure neutron matter and nearly symmetric nuclear matter in the absence of reliable microscopic calculations of the energy density of uniform nuclear matter at intermediate proton fractions. Better understanding of the equilibrium properties of neutron star matter at subnuclear densities will thus require future theoretical and/or experimental works covering the region of intermediate proton fractions.

4 Properties of phase transitions

The structural transitions examined in the previous section are first-order transitions. This is because the above-mentioned sequence of geometrical structure is mainly deter-

mined by the competition between the surface and Coulomb energies. In order to confirm this property, we have plotted in Fig. 4 the sizes of the nucleus or bubble and of the Wigner-Seitz cell, r_N and r_c , evaluated as functions of n_b for $C_1 = 400$ MeV fm 2 and $C_2 = 1.0$. It can be clearly seen from this figure that r_N and r_c jump at the transition points. It is of interest to note that for $C_2 = 0.01$, in which all the types of crystalline phases occur, the cell size r_c shows a dependence on the dimensionality d such that it is largest for $d = 3$ (spheres and spherical holes) and smallest for $d = 1$ (slabs). This behavior was also obtained from the previous liquid-drop-model calculations [4].

The neutron density profile is useful in probing how the system dissolves into uniform matter. In Fig. 5 we have thus plotted the neutron densities in the nuclear matter region and the neutron gas region for the crystalline phases as well as the one for the uniform phase, evaluated as functions of n_b for $C_1 = 300, 400, 500, 600$ MeV fm 2 and $C_2 = 1.0$. For these parameter sets, as shown in Fig. 3, there is a melting transition from the phase with slab-like nuclei to the uniform phase. We can observe from Fig. 5 that as the density approaches the melting point, the neutron distribution becomes more and more smooth. This behavior, as we have confirmed for various values of C_2 , is consistent with the results from the Thomas-Fermi calculations [5, 18]. We also find that at the melting point, the neutron density profile is discontinuous between the crystalline and uniform phases, indicating that the transition is of first order. However, this discontinuity should be fairly small as compared with the case of matter created in stellar collapse. In this case, due to larger proton fraction x yielded by degenerate neutrinos, such a discontinuity should become so large that neighbouring nuclei (or bubbles) appear to touch and fuse

with each other at the melting point. Detailed estimates made for this material will be reported elsewhere.

5 Thermal fluctuations

Let us now estimate thermally induced displacements of rod-like and slab-like nuclei from their equilibrium positions; the presence of these nuclei is energetically favored for typical values of C_1 and C_2 , as shown in Section 3. For such estimates, we first write the elastic constants for the phases containing these nuclei by following Pethick and Potekhin [11]. Since the phase with slab-like (rod-like) nuclei is structurally similar to a smectic A (columnar phase) liquid crystal, they derived the expressions for the elastic constants by comparing the energy increase due to deformation, obtained from the liquid-drop model for the nuclei in the incompressible limit, with that used for the corresponding liquid crystals. For the layered phase composed of slab-like nuclei, the energy density due to displacement v of layers in their normal direction (taken to be parallel to the z -axis) can be written as [19]

$$F = \frac{B}{2} \left[\frac{\partial v}{\partial z} - \frac{1}{2} (\nabla_{\perp} v)^2 \right]^2 + \frac{K_1}{2} (\nabla_{\perp}^2 v)^2. \quad (27)$$

Here, the elastic constants B and K_1 are expressed as [11]

$$B = 6w_{\text{C+L}}, \quad (28)$$

$$K_1 = \frac{2}{15} w_{\text{C+L}} (1 + 2u - 2u^2) r_{\text{c}}^2. \quad (29)$$

For the two-dimensional triangular lattice of rod-like nuclei, the energy density due to a two-dimensional displacement vector $\mathbf{v} = (v_x, v_y)$ of cylinders running along the z -axis is

given by [19]

$$\begin{aligned} F = & \frac{B}{2} \left(\frac{\partial v_x}{\partial x} + \frac{\partial v_y}{\partial y} \right)^2 + \frac{C}{2} \left[\left(\frac{\partial v_x}{\partial x} - \frac{\partial v_y}{\partial y} \right)^2 + \left(\frac{\partial v_x}{\partial y} + \frac{\partial v_y}{\partial x} \right)^2 \right] \\ & + \frac{K_3}{2} \left(\frac{\partial^2 \mathbf{v}}{\partial z^2} \right)^2 + B' \left(\frac{\partial v_x}{\partial x} + \frac{\partial v_y}{\partial y} \right) \left(\frac{\partial \mathbf{v}}{\partial z} \right)^2 + \frac{B''}{2} \left(\frac{\partial \mathbf{v}}{\partial z} \right)^4. \end{aligned} \quad (30)$$

Here, the elastic constants B , B' , B'' , C and K_3 read [11]

$$B = \frac{3}{2} w_{\text{C+L}}, \quad (31)$$

$$B' = -\frac{3}{4} w_{\text{C+L}}, \quad (32)$$

$$B'' = \frac{3}{8} w_{\text{C+L}}, \quad (33)$$

$$C \simeq 10^{2.1(u-0.3)} w_{\text{C+L}}, \quad (34)$$

$$K_3 \simeq 0.0655 w_{\text{C+L}} r_c^2 \quad (\text{for } 0.15 \lesssim u \lesssim 0.55). \quad (35)$$

In Eqs. (28), (29) and (31)–(35), $w_{\text{C+L}}$, as given by Eq. (8), satisfies the size-equilibrium condition (14).

We may then calculate the mean-square displacement at finite temperature T , defined as $\langle |v|^2 \rangle$, where $\langle \dots \rangle$ is the average over the probability distribution proportional to $\exp(-\int_V dV F/k_B T)$ with the lattice volume V and the Boltzmann constant k_B .² Let us assume that the length scale L of the lattice is far larger than r_c . For the one-dimensional

²Here the fluctuations are treated thermodynamically. At $T = 0$, however, the fluctuations behave quantum-mechanically; the resultant mean-square displacements are of order $\hbar c_2/(r_c^2 w_{\text{C+L}})$, where c_2 is the velocity of second sound associated with the varying inter-nuclear distance [20], roughly estimated as $c_2 \sim \sqrt{w_{\text{C+L}}/\rho_m}$. For typical values $r_c \sim 10$ fm, $w_{\text{C+L}} \sim 10^{-3}$ MeV fm $^{-3}$ and $\rho_m \sim 10^{14}$ g cm $^{-3}$, comparison of the quantum fluctuations thus estimated with the thermal fluctuations to be obtained below gives rise to the quantum-classical crossover temperature of order 10^7 K for planar nuclei and of order 10^8 K for cylindrical nuclei. Consequently, the forthcoming arguments hold good for $T \gtrsim T_0$ but underestimate the displacement for $T \lesssim T_0$.

layered lattice, the mean-square displacement can then be evaluated within the harmonic approximation allowing for the terms up to $O(v^2)$ in Eq. (27) as [20]

$$\langle |v|^2 \rangle \simeq \frac{k_B T}{4\pi\sqrt{BK_1}} \ln\left(\frac{L}{a}\right), \quad (36)$$

where $a = 2r_c$ is the layer spacing. For the two-dimensional triangular lattice, by retaining the terms up to $O(v_x^2)$ and $O(v_y^2)$ in Eq. (30), we obtain [20]

$$\langle |\mathbf{v}|^2 \rangle \simeq \frac{k_B T}{(B+2C)\sqrt{\pi\lambda a}}, \quad (37)$$

where $\lambda = \sqrt{2K_3/(B+2C)}$, and $a = (2\pi/\sqrt{3})^{1/2}r_c$ is the lattice constant for hexagonal cells.³ Expressions (36) and (37) are analogous to those appearing in the context of Landau-Peierls instabilities, which destroy a one-dimensional ordering in an *infinite* three-dimensional system.

In Fig. 6 (7) we have plotted the ratio $\sqrt{\langle |\mathbf{v}|^2 \rangle}/(a/2 - r_N)$ of the root-mean-square displacement of the slab-like (rod-like) nucleus, calculated from Eq. (36) [(37)] for $k_B T = 0.1$ MeV, to the shortest distance between the surface of the nucleus in its equilibrium position and the boundary of the cell containing it. In these calculations we have set $L = 10$ km, which is the typical neutron star radius. The results for the layered phase, depending on L logarithmically, are essentially unchanged by the choice of L ; when we set $L = 1$ μm , for example, the values shown in Fig. 6 are only multiplied by a factor of $\simeq 0.7$. It is obvious from comparison between Figs. 6 and 7 that for the same C_1 and C_2 the relative displacement of the slab-like nucleus is appreciably large compared

³Strictly speaking, Eq. (37) is valid when the length of the nuclei is large compared with the linear dimension of the lattice in the xy plane. This situation is energetically preferred over the opposite case, in which there is a larger total sectional area of the nuclei at the boundary of the lattice.

with that of the rod-like nucleus, a feature yielded by the logarithmic factor appearing in Eq. (36). We also find that the relative displacement for both lattices decreases with increasing surface tension (or C_2). This is because the elastic constants, acting to reduce the displacements given by Eqs. (36) and (37), are proportional to the equilibrium value of w_{C+L} satisfying condition (14).

It is noteworthy that for the typical parameter set ($C_1 = 400$ MeV fm 2 and $C_2 = 1.0$), the relative displacement for the layered phase at $k_B T = 0.1$ MeV, as plotted in Fig. 6, takes on values of up to about unity. The planar nucleus deformed to such an extent touches the boundary of the neighbouring cell as defined in the case in which the lattice is in its equilibrium. This suggests the possibility that the fluctuational displacements destroy the ordered configuration in a length scale of down to $\sim r_c$ even at temperatures typical of matter in the neutron star crust.⁴ In theoretically predicting the interiors of observed neutron stars having various temperature profiles, therefore, it is useful to estimate as a function of n_b the critical temperature T_c at which the relative displacements become unity. The results obtained for the layered lattice and the triangular lattice have been plotted in Figs. 8 and 9, respectively.⁵ The difference in T_c between these two lattices, as can be observed from Figs. 8 and 9, suggests that if formation of these two lattices can occur dynamically in the star, the layered phase is formed later than the triangular phase during the star's cooling.

⁴ Reconnection of the planar nuclei that may be involved in such destruction leads inevitably to departures from thermodynamic equilibrium, which are beyond the scope of this paper.

⁵ Note that the values of T_c are meaningless when they are smaller than the crossover temperature T_0 from the classical to the quantum fluctuations; in this case, quantum effects keep the relative displacement large compared with unity for $T < T_0$.

6 Conclusion

We have examined the dependence on the surface tension E_{surf} and on the proton chemical potential $\mu_p^{(0)}$ in pure neutron matter, of the density region in which the presence of non-spherical nuclei and of bubbles is energetically favored at $T = 0$. We have found that as E_{surf} decreases or $\mu_p^{(0)}$ increases, such a density region becomes larger. For the values of E_{surf} and $\mu_p^{(0)}$ as adopted in recent literature, our results show that in the ground state, the phases with rod-like nuclei and with slab-like nuclei lie between the bcc lattice phase and the uniform nuclear matter phase. The fluctuational displacements of such non-spherical nuclei from their equilibrium positions have been estimated at finite temperature. It has been suggested that at temperatures typical of matter in the neutron star crust, such fluctuations may melt the layered lattice of slab-like nuclei.

Even if rod-like and slab-like nuclei are thermodynamically stable, whether or not they are actually present in the star depends on occurrence of the dynamical processes leading to their formation. These processes are thought to involve instabilities against nuclear deformation and against proton clustering in uniform nuclear matter [1]. If the occurrence of such processes were confirmed, it would become still more significant to consider effects of the presence of non-spherical nuclei on the structure and evolution of neutron stars. In the context of pulsar glitches, the question of what kind of impurities and defects are formed in the lattices of non-spherical nuclei would be essential to understanding of the mechanism for neutron vortex pinning. For neutron star cooling, it would be interesting to consider the direct URCA processes in non-spherical nuclei; as suggested by Lorenz et al. [4], these processes might be allowed by the proton continuous spectrum in the

elongated direction of the nuclei, in contrast to the case of roughly spherical nuclei, and by the band structure of neutrons moving in the periodic potential created by the nuclei.

Acknowledgements

We are grateful to Professor Takeo Izuyama for useful discussion and valuable comments. This work was supported in part by Grants-in-Aid for Scientific Research provided by the Ministry of Education, Science and Culture of Japan through Research Grant No. 07CE2002 and No. 10-03687.

References

- [1] C.J. Pethick and D.G. Ravenhall, Annu. Rev. Nucl. Part. Sci. 45 (1995) 429.
- [2] D.G. Ravenhall, C.J. Pethick and J.R. Wilson, Phys. Rev. Lett. 50 (1983) 2066.
- [3] M. Hashimoto, H. Seki and M. Yamada, Prog. Theor. Phys. 71 (1984) 320.
- [4] C.P. Lorenz, D.G. Ravenhall and C.J. Pethick, Phys. Rev. Lett. 70 (1993) 379.
- [5] K. Oyamatsu, Nucl. Phys. A561 (1993) 431.
- [6] K. Sumiyoshi, K. Oyamatsu and H. Toki, Nucl. Phys. A 595(1995)327.
- [7] M. Ruderman, in *Unsolved Problems in Astrophysics*, eds. J.N. Bahcall and J.P. Ostriker (Princeton Univ. Press, Princeton, New Jersey, 1997), p. 281.
- [8] P.B. Jones, Mon. Not. R. Astron. Soc. 296 (1998) 217; Mon. Not. R. Astron. Soc. 306 (1998) 327; Phys. Rev. Lett. 83 (1999) 3589.
- [9] J. Arponen, Nucl. Phys. A191(1972)257.
- [10] G. Baym, H.A. Bethe and C.J. Pethick, Nucl. Phys. A175 (1971)225.
- [11] C.J. Pethick and A.Y. Potekhin, Phys. Lett. B427 (1998) 7.
- [12] H.M. Van Horn, Science 252 (1991) 384.
- [13] C.J. Pethick, D.G. Ravenhall and C.P. Lorenz, Nucl. Phys. A584 (1995) 675.
- [14] P.J. Siemens and V.R. Pandharipande, Nucl. Phys. A173 (1971) 561.

- [15] O. Sjöberg, Nucl. Phys. A222 (1974) 161.
- [16] D.G. Ravenhall, C.D. Bennett and C.J. Pethick, Phys. Rev. Lett. 28 (1972) 978.
- [17] K. Iida and K. Sato, Astrophys. J. 477 (1997) 294.
- [18] R. Ogasawara and K. Sato, Prog. Theor. Phys. 71 (1984) 320.
- [19] P.G. de Gennes and J. Prost, *The Physics of Liquid Crystals*, 2nd ed. (Clarendon, Oxford, 1993).
- [20] S. Chandrasekhar, *Liquid Crystals*, 2nd ed. (Cambridge Univ. Press, Cambridge, 1992).

Fig. 1. The proton chemical potential in pure neutron matter as a function of neutron density. The thick lines are the results calculated from Eq. (4) for $C_1 = 300, 400, 600$ MeV fm 2 . The thin broken lines as marked by the Skyrme interactions (FPS21, 1', FPS and SkM) are the results summarized by Pethick, Ravenhall and Lorenz [13], and the thin solid line is the result of Sjöberg [15]. The crosses denote the values obtained by Siemens and Pandharipande [14].

Fig. 2. The surface energy per unit area (the surface tension) as a function of x , the proton fraction in the nuclear matter region. The thick broken curves are the present results obtained from Eq. (6) for $C_1 = 400$ MeV fm 2 and $C_2 = 0.01, 0.1, 1.0, 2.5, 5.0$, the solid curve is the RBP result from their Hartree-Fock calculations [16], and the dotted curve is the BBP result [10].

Fig. 3. Zero-temperature phase diagrams on the n_b versus C_2 plane, evaluated for $C_1 = 300, 400, 500, 600$ MeV fm 2 .

Fig. 4. Size of a nucleus or bubble, r_N , and of a Wigner-Seitz cell, r_c , calculated for $C_1 = 400$ MeV fm 2 and $C_2 = 0.01, 1.0, 2.5$ as a function of baryon density n_b . The symbols SP, C, S, CH and SPH stand for sphere, cylinder, slab, cylindrical hole and spherical hole, respectively.

Fig. 5. The neutron densities obtained for $C_1 = 300, 400, 500, 600$ MeV fm 2 and $C_2 = 1.0$ as functions of baryon density n_b . The lines classified by $[n(1 - x)]_N$ and n_n represent the neutron densities in the nuclear matter region and in the neutron gas region for the phases with nuclei, respectively. The lines classified by $[n(1 - x)]_{\text{uni}}$ denote the neutron densities in uniform nuclear matter.

Fig. 6. The root-mean-square displacement of a planar nucleus at $k_B T = 0.1$ MeV, divided by the shortest distance between the surface of the nucleus in its equilibrium position and the boundary of the cell containing it. The curves are obtained for various sets of C_1 and C_2 as a function of baryon density n_b . The thick curves lying between the two vertical lines are the results in the density region in which the phase with planar nuclei is energetically stable.

Fig. 7. The root-mean-square displacement of a cylindrical nucleus at $k_B T = 0.1$ MeV, divided by the distance between the surface of the nucleus in its equilibrium position and the boundary of the cell containing it. The curves are obtained for various sets of C_1 and C_2 as a function of baryon density n_b . The thick curves lying between the two vertical lines are the results in the density region in which the phase with cylindrical nuclei is energetically stable.

Fig. 8. The critical temperature T_c for the phase with planar nuclei as a function of baryon density n_b . The thick curves lying between the two vertical lines are the results in the density region in which the phase with planar nuclei is energetically stable.

Fig. 9. The critical temperature T_c for the phase with cylindrical nuclei as a function of baryon density n_b . The thick curves lying between the two vertical lines are the results in the density region in which the phase with cylindrical nuclei is energetically stable.

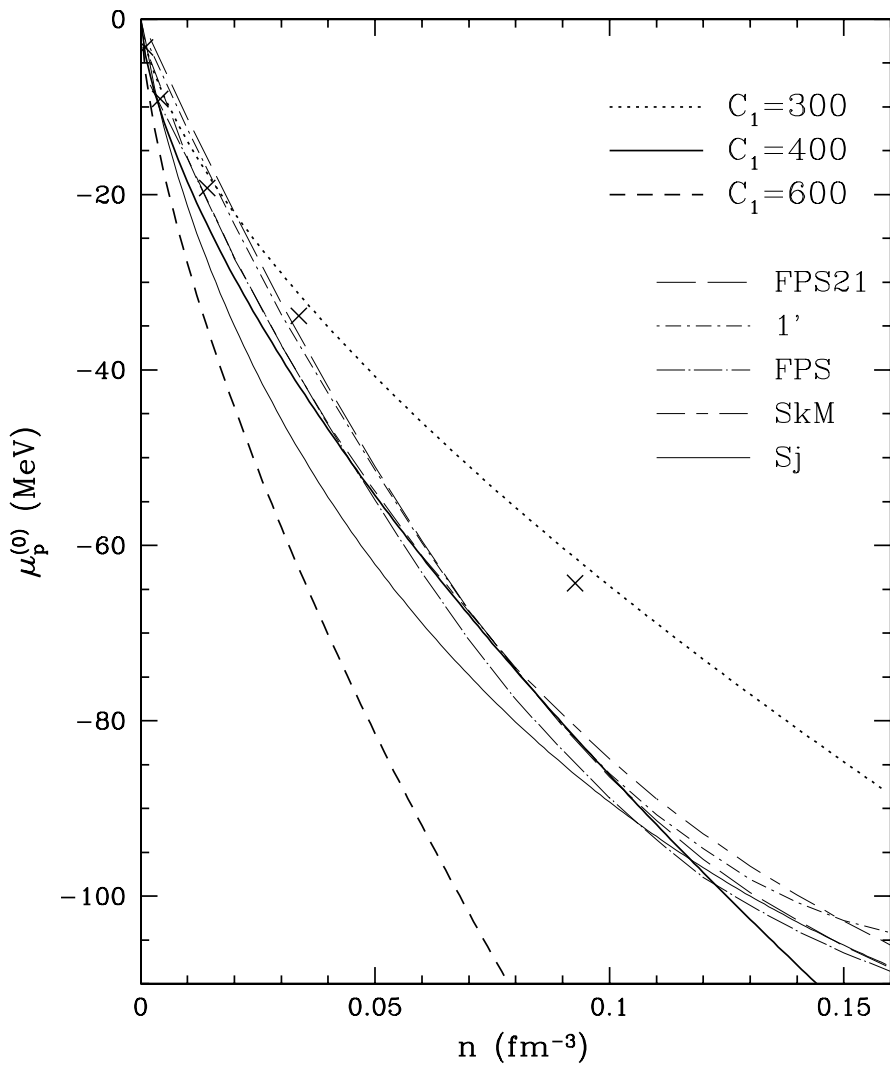


Figure 1:

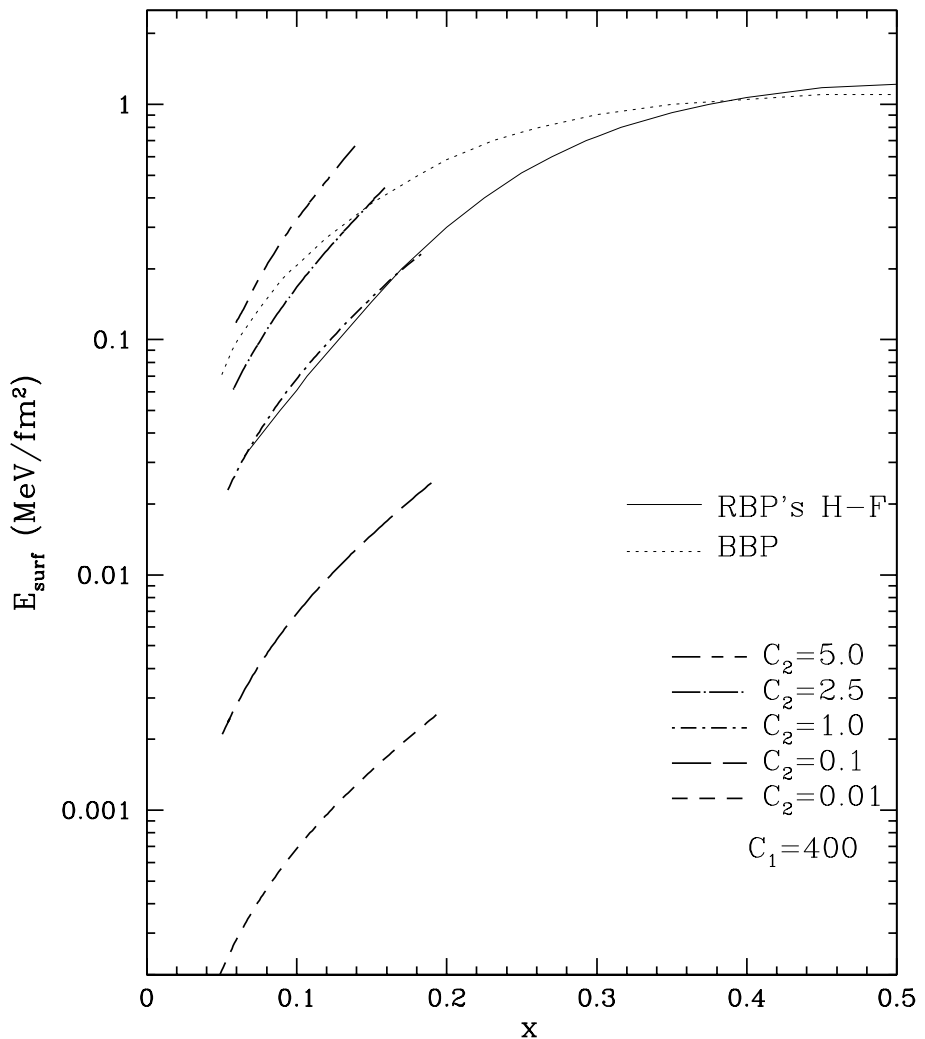


Figure 2:

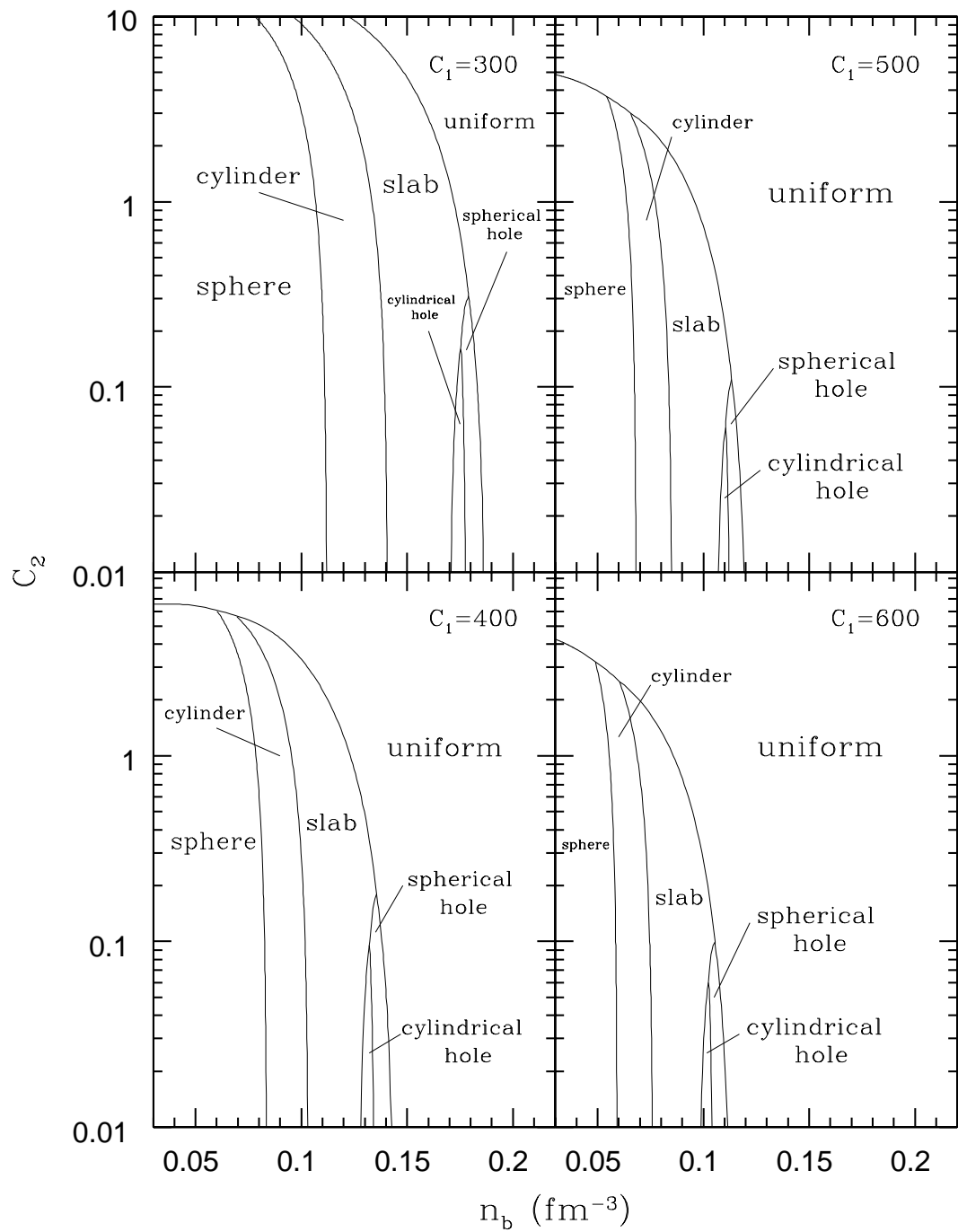


Figure 3:

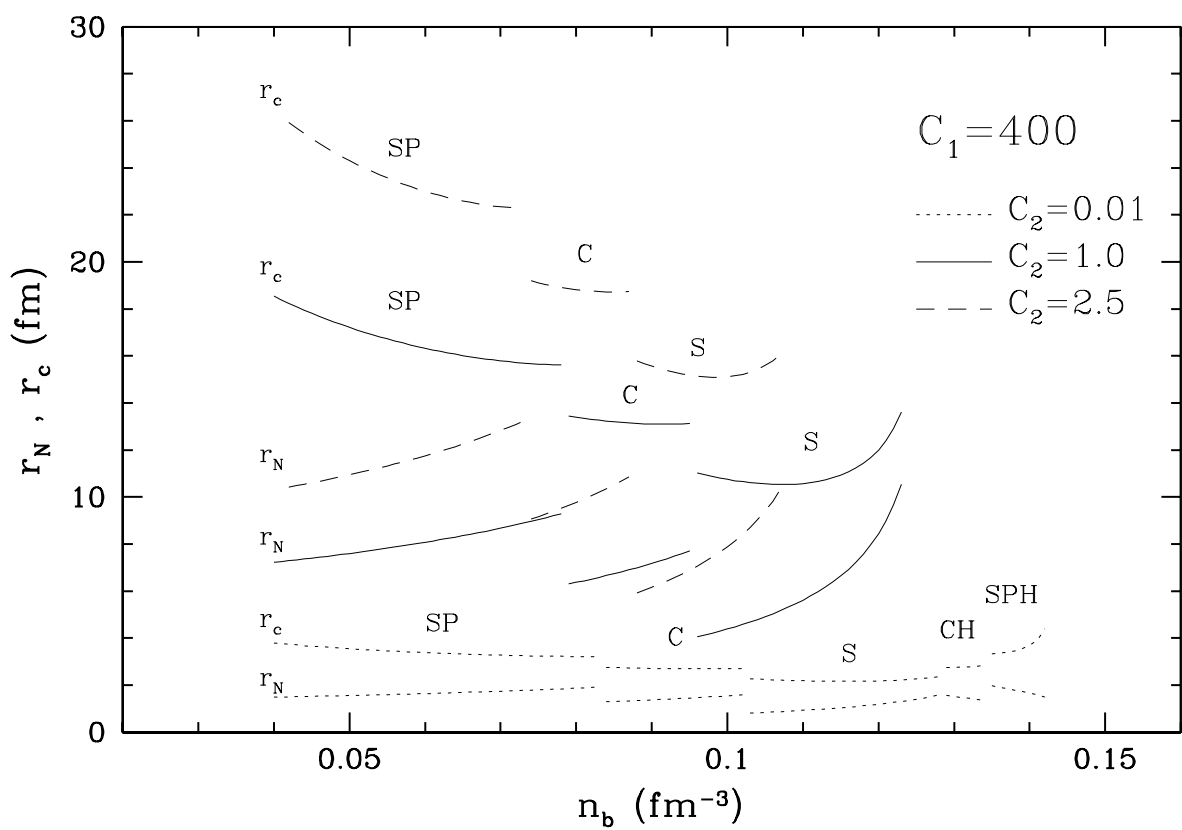


Figure 4:

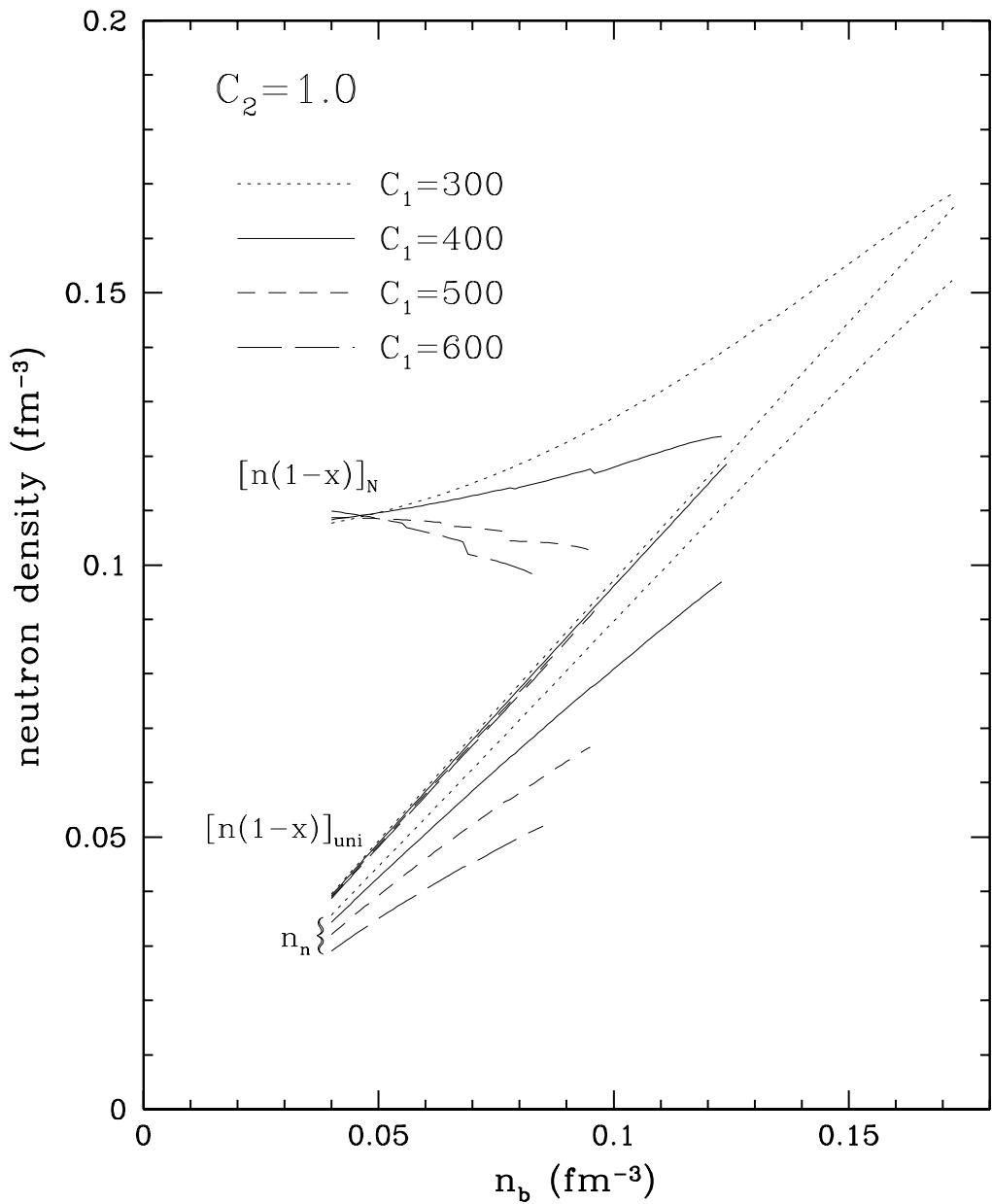


Figure 5:

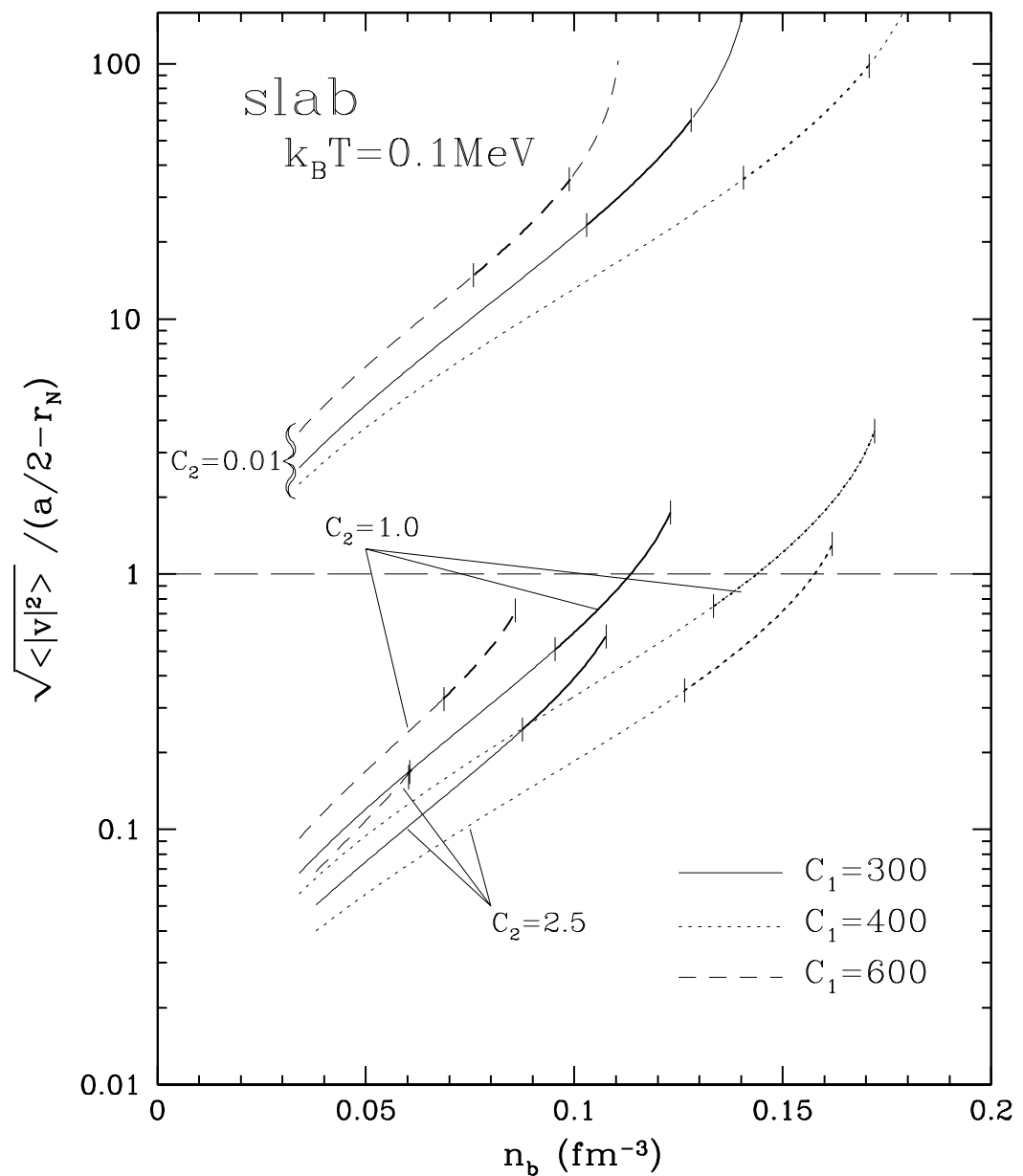


Figure 6:

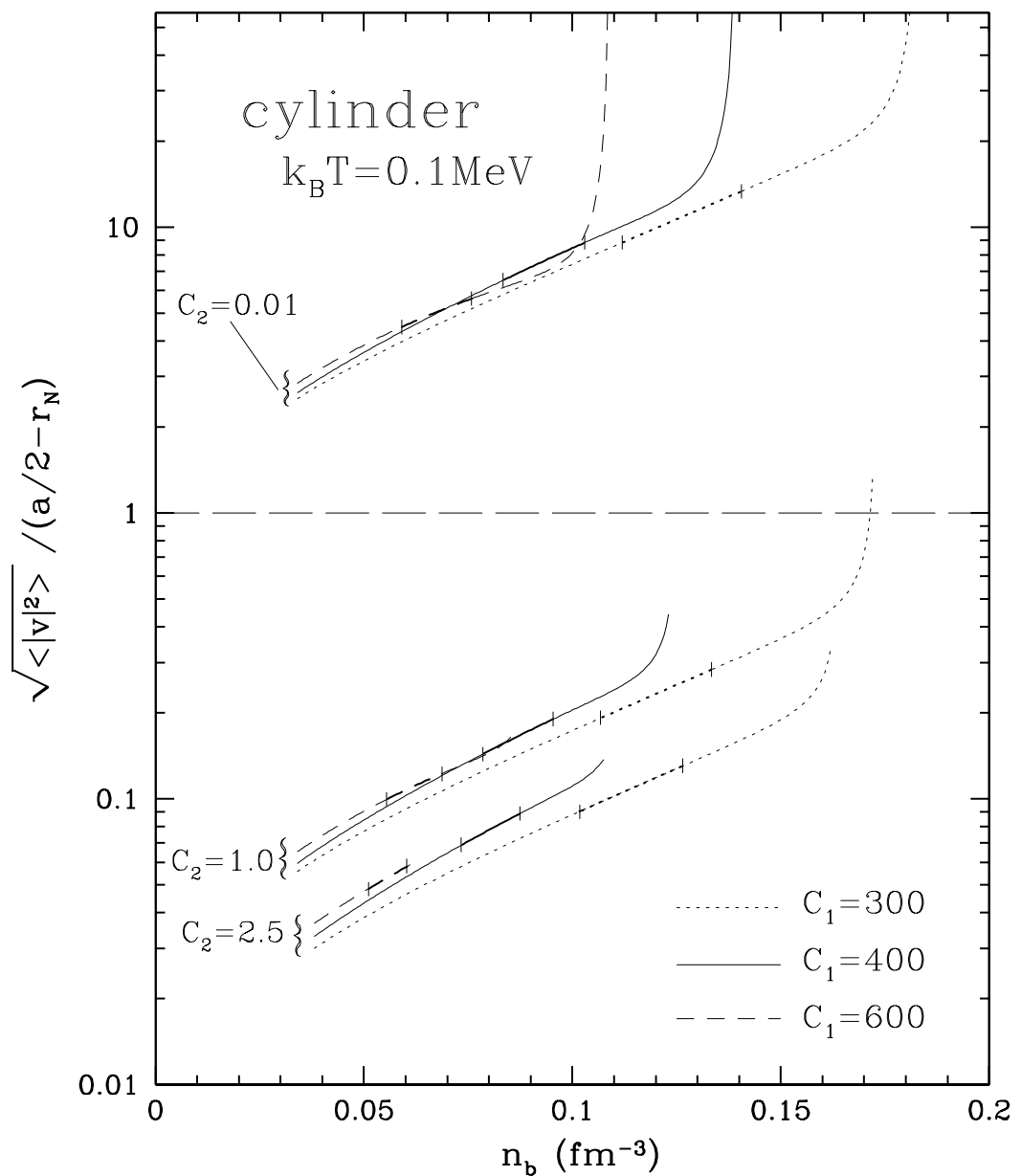


Figure 7:

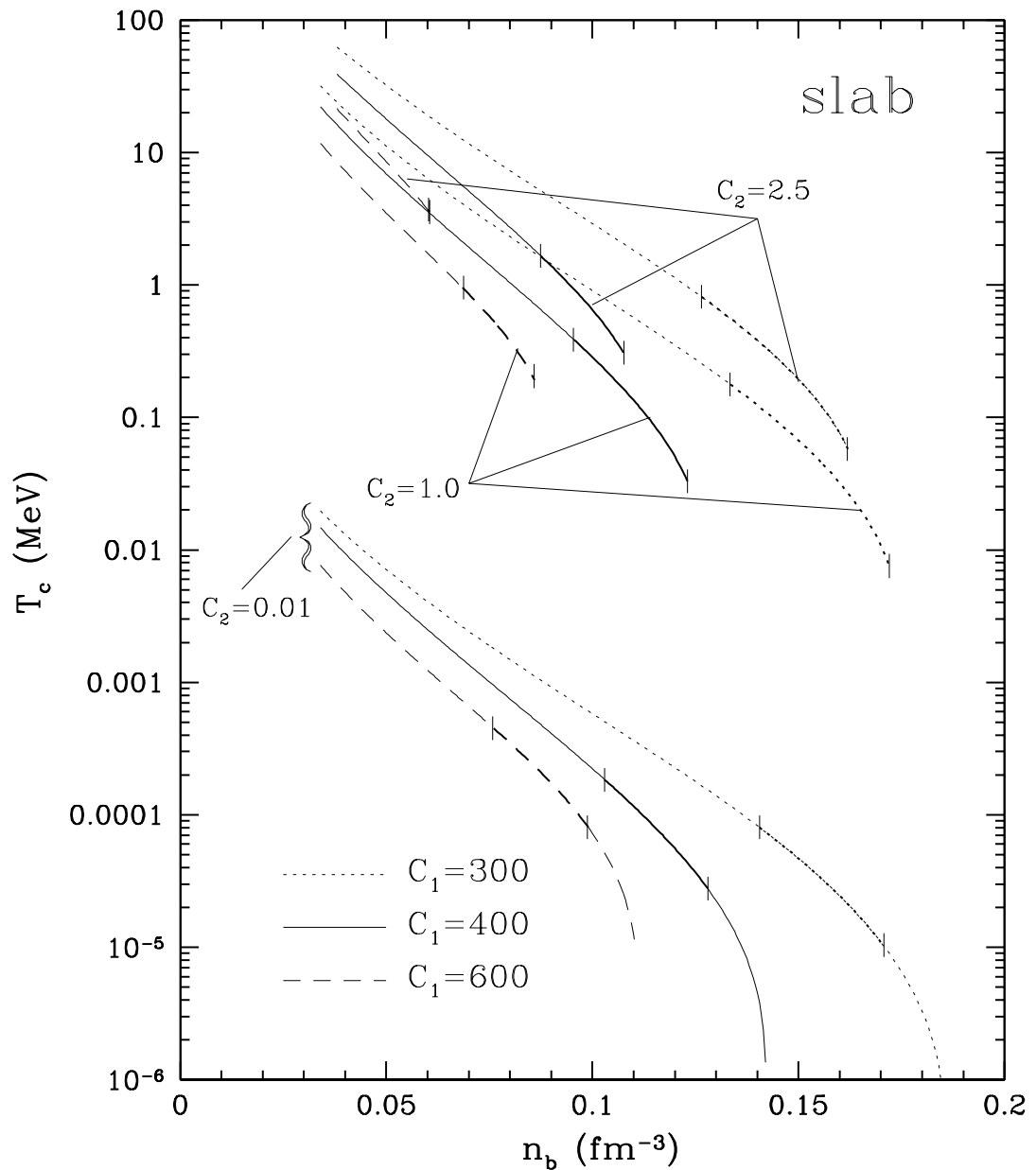


Figure 8:

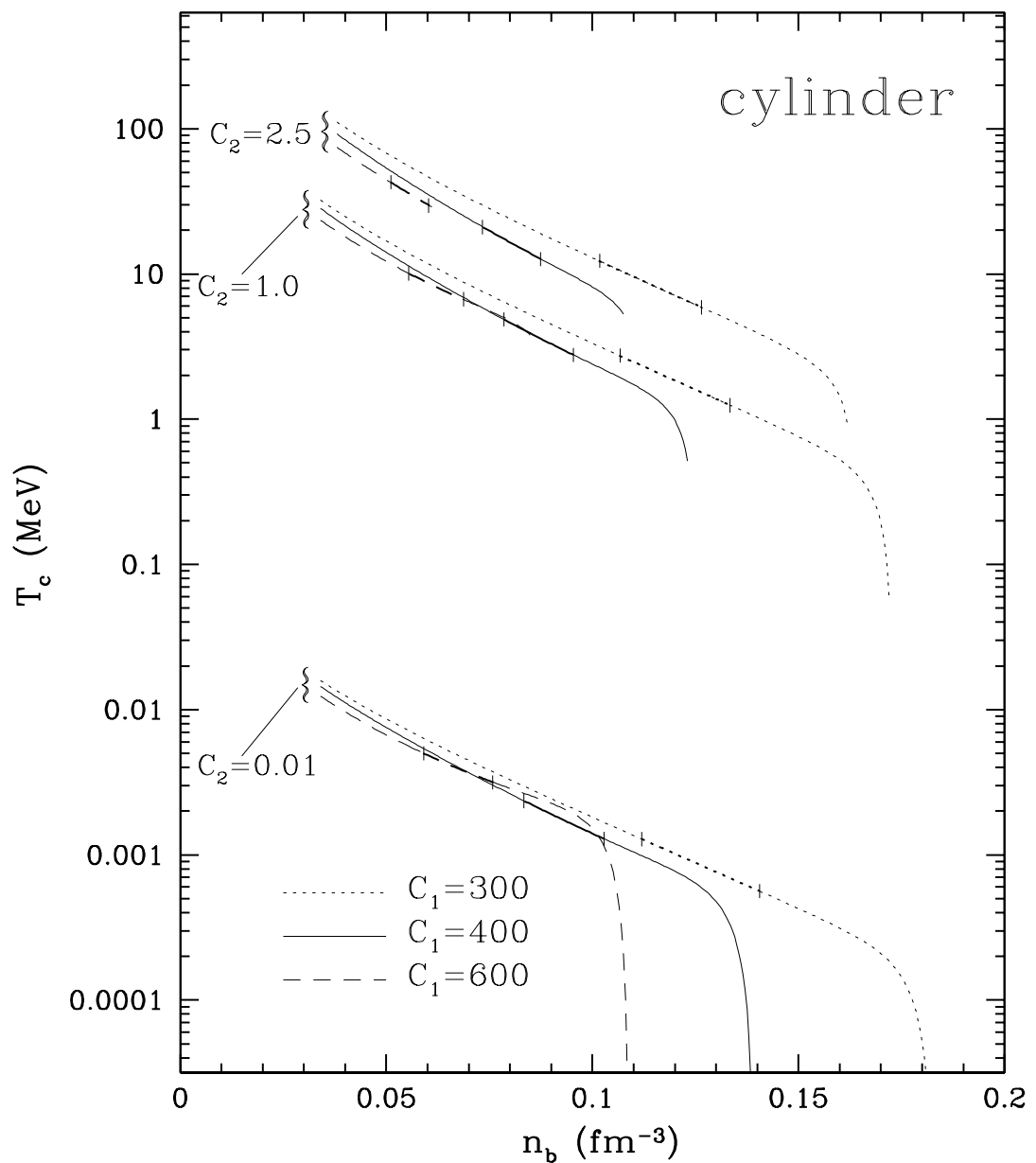


Figure 9: